Ordering process and Bloch wall dynamics in a two-dimensional anisotropic spin system

Hiroki Tutu
Department of Physics, Kyushu University 33, Fukuoka 812, Japan
(Received 3 June 1997)

The ordering process of a nonconserved anisotropic XY-spin system in two-dimensional space is investigated. The dynamics is described by the motion of the domain wall, the so-called Bloch wall, which has chirality, in addition to the curvature of the interface. We obtain a convenient description for the dynamics of the domain wall, which has a generalized form of the Allen-Cahn-type equation of motion for the phase boundary, taking into account the effect of the width of the wall. We also discuss the short-scale behavior of the correlation function for this system when the system relaxes from an $O(2)$ symmetry state to a state having $O(1)$ symmetry. [S1063-651X(97)12710-6]

PACS number(s): 05.70.Ln, 64.60.Cn, 75.60.Ch

I. INTRODUCTION

The ordering process, where defects play an important role, has been extensively investigated [1]. In particular the research for a system having $O(n)$ symmetry has a history [2–6]. For an extension of these problems, we consider an anisotropy-induced system on an isotropic system. This system may have more of a variety of pattern-forming dynamics and kinetic stages of ordering dynamics than the symmetric $O(n)$ system. Considering the uniaxial anisotropy, one of the roles of this anisotropy is to split approximately the order-parameter-space into the product space of some partial order parameter-spaces. For example an n-vector system induced by one anisotropy axis has the space $O(1)\times O(n-1)$ at most. In such a system one can expect the coexistence of varieties of topological defects and the coupling of dynamics among them. We will discuss these in the frame of the nonconserved time-dependent Ginzburg-Landau dynamics.

In the present paper we study the two-dimensional anisotropic XY spin system after a quench from an unstable uniform disordered phase to a stable ordered one. We have investigated from both dynamical and statistical viewpoints, focusing on the dynamical regime driven by defects.

Due to its symmetry, this system has an interface separating two stable phases. In the regions where the anisotropy is not so strong, it is known that the interface has a Bloch wall structure. With a purely mechanical approach, we have derived that the reduced dynamics for the interface consists of Bloch walls. We have obtained similar results to what is known for the interface dynamics for the scaler-order parameter system, the so called Allen-Cahn equation [7], but which includes some slightly new features.

We have also investigated the behavior of the correlation function on a small scale, both numerically and theoretically. We will discuss the crossover behavior for that in the assumption that the system reduces its symmetry dynamically from $O(2)$ to $O(1)$, utilizing results obtained from our interface approach, and a general consequence for the correlation function of the $O(n)$ system obtained by Ohta, Jasnow, and Kawasaki, and Tomita, Toyoki, and Bray.

This paper is organized as follows. In Sec. II we present the model. In Sec. III we obtain the fundamental equations controlling the interface dynamics for this system. In Sec. IV we discuss the crossover behavior of the correlation function. We then summarize all the results in Sec. V.

II. MODEL

Let us consider the Ginzburg-Landau free energy with anisotropy in two-dimensional space [8,9],

$$H\{\psi,\psi^*\}=\int\left\{-|\psi|^2+\tfrac{1}{2}|\psi|^4-\frac{\gamma}{2}(\psi^2+\psi^{*2})+|\nabla\psi|^2\right\}d\boldsymbol{r}, \tag{2.1}$$

where ψ is a complex order parameter, and γ is the strength of the anisotropy. The third term in the integrand represents the anisotropic energy, which produces a preferred direction in the circular order-parameter space.

We consider the time development of the order parameter, which represents a nonconservative anisotropic XY-spin system. Using the free energy Eq. (2.1), let us assume that the evolution of $\psi(x,t)$ obeys

$$\partial_t\psi(\boldsymbol{r},t)=-\frac{\delta H\{\psi,\psi^*\}}{\delta\psi^*(x,t)}=\psi-|\psi|^2\psi+\gamma\psi^*+\nabla^2\psi, \tag{2.2}$$

where the parameters and the variable have been scaled appropriately, and we have neglected random force.

This system has discrete uniform states for nonzero γ, which is taken to be positive without generality. The stable uniform states are $\psi=\pm\sqrt{1+\gamma}$, and the unstable uniform states are $\psi=0$ and $\pm i\sqrt{1-\gamma}$ for γ smaller than unity γ (<1).

As is well known, the above system has two types of domain wall solutions [10], Ising and Bloch walls. Varieties of the wall structure result from the competition between the anisotropy and the elasticity, i.e., the third and fourth terms in the free energy Eq. (2.1). Both walls are also very familiar in liquid-crystal systems [11]. The Ising (Néel) wall is given by

$$\psi_I(\boldsymbol{r})=\pm\sqrt{1+\gamma}\tanh[\boldsymbol{n}\cdot(\boldsymbol{r}-\boldsymbol{r}_0)/\xi_I], \tag{2.3}$$

where + (−) stands for the kink (antikink) which is located at the position $\boldsymbol{r}_0$, and has the interface normal to the unit vector $\boldsymbol{n}$ and the width $\xi_I=\sqrt{1+\gamma}/\sqrt{2}$. This solution is stable for $\gamma>\frac{1}{3}$. Because of the strong anisotropy, the order parameter vanishes at the center of the wall.

On the other hand, the Bloch wall stably exists for $\gamma<\frac{1}{3}$ and takes the form

$$\psi_B(\boldsymbol{r})=pX[\boldsymbol{n}\cdot(\boldsymbol{r}-\boldsymbol{r}_0)/\xi_B]+iqY[\boldsymbol{n}\cdot(\boldsymbol{r}-\boldsymbol{r}_0)/\xi_B], \tag{2.4}$$

where $X(x)=X_0\tanh(x)$, $Y(x)=Y_0\,\mathrm{sech}(x)$ $(X_0=\sqrt{1+\gamma}$, $Y_0=\sqrt{1-3\gamma})$, $\xi_B=1/\sqrt{2\gamma}$ is the width of the interface, and both p and q take either $+1$ or -1. Here the sign of q represents the chirality of the wall [10]. Walls with different chilarity have equal stability. In contrast to the Ising wall, the order parameter does not vanish at the Bloch wall, since the anisotropic energy is weaker than the elastic energy.

In a previous work [12] we investigated the one-dimensional version of Eq. (2.2). In that system the degree of freedom for the chilarity on the Bloch wall plays a special role. Let q_i be the sign of q at the ith Bloch wall. The quantity $\Sigma_i(-1)^i q_i$ turns out to be a conservative quantity in the course of time. Due to this conservation law, the assembly of Bloch walls eventually forms a corkscrew structure. This is a particular characteristic in the one-dimensional system. In the present two-dimensional system, however, there is no such particular structure so long as we use the usual periodic boundary condition. In Sec. III we derive the dynamics for Bloch walls by generalizing to the curved interface and by introducing space-dependent chirality.

III. BLOCH WALL DYNAMICS

The interface dynamics for conserved and nonconserved one-component order parameter system has been developed by Lifshitz [13], Allen and Cahn [7], and Kawasaki and Ohta [14]. It gives reduced information about how interfaces develop in the course of an ordering process. We can continue to investigate the present system along the lines of the above works.

For the interface formed by Ising walls for $\gamma>\frac{1}{3}$, the interface dynamics gives the same results mentioned above, since such system is considered to be effectively one-component system. Thus we focus our attention on the regime $0<\gamma<\frac{1}{3}$, where the Bloch wall is stable. Let us refer to regions with Re $\psi=0$ as *interfaces*, and regions with $\psi\approx 0$ as *defects*.

Figure 1 shows characteristic patterns of $\psi(\boldsymbol{r},t)$ for $\gamma=0.03$ at two different times denoted 1 (earlier time, $t=196$) and 2 (later time, $t=416$), and that for two different quantities denoted Figs. 1(a1), and 1(a2) for amplitude $|\psi|$ and Figs. 1(b1) and 1(b2) for corresponding Im ψ. Here we have numerically solved Eq. (2.2) by using the explicit Euler scheme on a two-dimensional square with the periodic boundary condition. The numerical calculation has been carried out on a square of size 512×512 , with a discritized time step 0.02 and a spatial mesh size 0.5, using initial conditions $|\psi|\approx10^{-3}$.

In view of Fig. 1(a), there are interfaces which separate two phases $\psi=\sqrt{1+\gamma}$ and $\psi=-\sqrt{1+\gamma}$ regions. Furthermore, each interface contains defects with even numbers, which annihilate by the collision with each other in the course of time. Alternative views of Fig. 1(b) show the manner in which segments (bright or dark region) on an interface shrink and disappear successively.

Let us consider an interface located at $\boldsymbol{r}_0\equiv\boldsymbol{r}_0(s,t)$, where s is the arclength. Here we consider the late stage dynamics, in which the curvatures of interfaces are sufficiently smooth and all interfaces can be treated independently. In the vicinity of the interface the order parameter can be written in the form of Eq. (2.4). Let us introduce a continuous variable $q(\boldsymbol{r},t)$ instead of q in Eq. (2.4). Thus we assume the following-order parameter profile:

$$\psi(\boldsymbol{r},t)=X[\boldsymbol{n}(s,t)\cdot(\boldsymbol{r}-\boldsymbol{r}_0)/\xi_B] + iq(\boldsymbol{r},t)Y[\boldsymbol{n}(s,t)\cdot(\boldsymbol{r}-\boldsymbol{r}_0)/\xi_B], \tag{3.1}$$

where $q(\boldsymbol{r},t)$, which will be denoted as q, is a real variable. q parametrizes the chirality of the Bloch wall and takes values $q\simeq\pm1$ in regions except for defects, signs corresponding to the right- or left-hand rotation of a wall. $\boldsymbol{n}(s,t)$ is the unit normal vector to the interface located at $\boldsymbol{r}_0(s,t)$ (Fig. 2). However, the above representation is not complete, since the width of wall is not a constant. To take into account the width of wall, Eq. (3.1) is generalized into

$$\psi(\boldsymbol{r},t)=X[\,\eta(\boldsymbol{r},t)/\xi_B]+iq(\boldsymbol{r},t)Y[\,\eta(\boldsymbol{r},t)/\xi_B], \tag{3.2}$$

with a position-dependent variable $\eta(\boldsymbol{r},t)$. One finds that $\eta(\boldsymbol{r},t)$ represents the distance from an interface. Furthermore, let us introduce the metric $g_\eta\equiv g_\eta(\boldsymbol{r},t)\equiv\nabla\eta\cdot\nabla\eta$. Here g_η takes unity except near defects $(q\sim0)$. One easily finds the relation

$$\eta(\boldsymbol{r},t)\equiv\int_{\boldsymbol{r}_0}^{\boldsymbol{r}}\sqrt{g_\eta}\,\boldsymbol{n}(\boldsymbol{x},t)\cdot d\boldsymbol{x}. \tag{3.3}$$

We will find the relation between the metric g_η and the variable q later.

The substitution of Eq. (3.2) into Eq. (2.2), by treating the real and imaginary parts separately, leads to a pair of equations of motion for the interface as

$$\partial_t\eta=\xi_B\tanh(\,\eta/\xi_B)(1+\gamma-4\gamma g_\eta-Y_0^2q^2)+\nabla^2\eta, \tag{3.4}$$

$$\partial_t q=(1-\gamma-2\gamma g_\eta-Y_0^2q^2)q+\nabla^2q - (2/\xi_B)\tanh(\,\eta/\xi_B)\nabla q\cdot\nabla\eta. \tag{3.5}$$

To extract useful results from the above equations, we assume the temporal evolution of η in Eq. (3.4) can be regarded as quasistatic. This assumption is well satisfied so long as we are concerned with the smooth interface.

Taking gradients of both sides of Eq. (3.4) with the use of $\nabla\eta=\sqrt{g_\eta}\boldsymbol{n}$, and an operating inner product with a unit normal vector $\boldsymbol{n}$ and a unit tangent vector $\boldsymbol{t}$ separately to it, we obtain the following pair of equations:

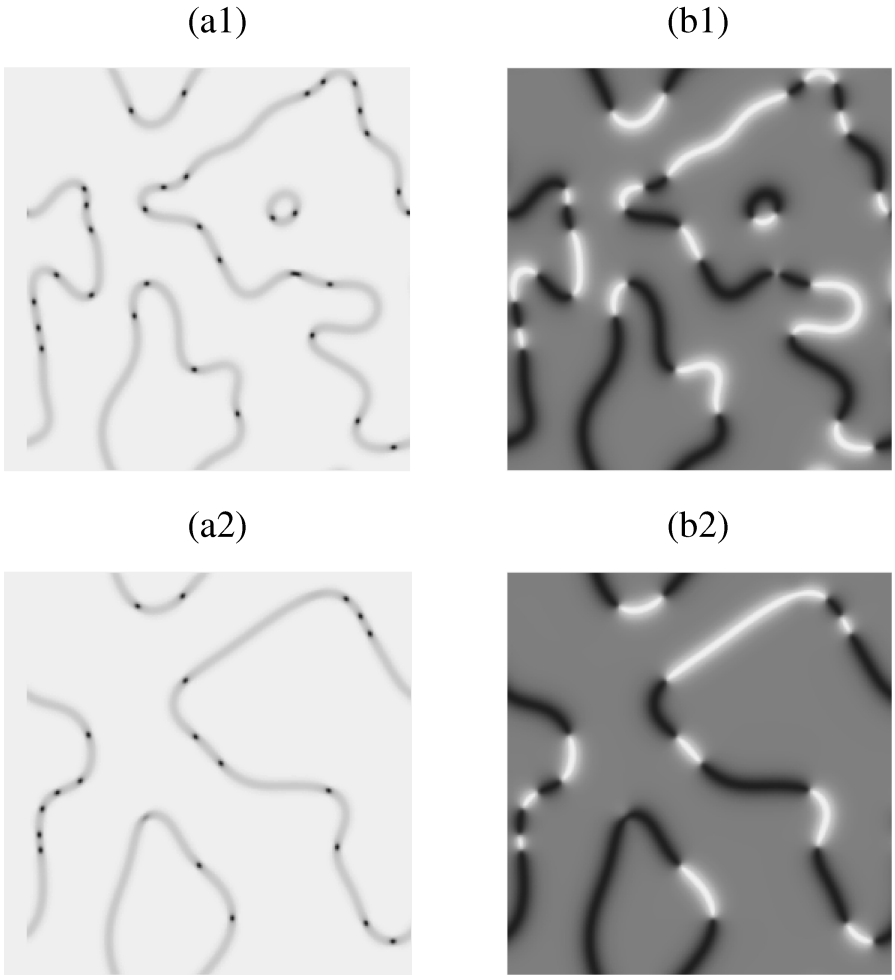

FIG. 1. Temporal evolution of the $\psi(\mathbf{r},t)$. (a1) and (a2) show patterns of amplitude $|\psi|$ for different times $t=196$ (a1) and $t=416$ (a2). (b1) and (b2) show same-time patterns of (Imψ) of (a1) and (a2), respectively. The patterns in (a1) and (a2) consist of interfaces (the gray region) which separate the two phases (bright region) and the defects (black region). Patterns in (b1) and (b2) consist of segments of black and white regions corresponding to the opposite chirality on the interface.

$$\partial_t\sqrt{g_\eta}=\mathrm{sech}^2(\eta/\xi_B)(1+\gamma-4\gamma g_\eta-Y_0^2q^2)\sqrt{g_\eta}-\xi_B\tanh(\eta/\xi_B)(4\gamma\boldsymbol{n}\cdot\nabla g_\eta+Y_0^2\boldsymbol{n}\cdot\nabla q^2)-(\nabla\theta)^2\sqrt{g_\eta}+\nabla^2\sqrt{g_\eta}, \tag{3.6}$$

$$\sqrt{g_\eta}\partial_t\theta=-\xi_B\tanh(\eta/\xi_B)(4\gamma\boldsymbol{t}\cdot\nabla g_\eta+Y_0^2\boldsymbol{t}\cdot\nabla q^2)+2\nabla\sqrt{g_\eta}\cdot\nabla\theta+\sqrt{g_\eta}\nabla^2\theta, \tag{3.7}$$

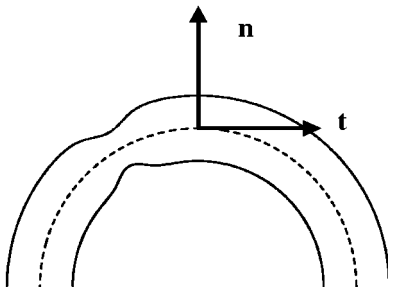

FIG. 2. The geometry of the interface. Dashed and solid lines denote the interface defined by Re $\psi=0$, and the width of wall associated with it, respectively.

where θ is the directional angle defined via $\boldsymbol{n}\equiv(\cos\theta,\sin\theta)$ and $\boldsymbol{t}\equiv(-\sin\theta,\cos\theta)$. Since we focus our attention on the interface $\eta\sim0$ ($\boldsymbol{r}\sim\boldsymbol{r}_0$), we then multiply $\tanh'(\eta/\xi_B)$ to Eqs. (3.6) and (3.7), and integrate them with respect to η/ξ_B by neglecting the η dependence in g_η, q, θ, and $\boldsymbol{n}$ by assuming a weak dependence of them on η. We obtain the reduced equations

$$\partial_t\sqrt{g_\eta}=\frac{1}{C}(1+\gamma-4\gamma g_\eta-Y_0^2q^2)\sqrt{g_\eta}-(\nabla\theta)^2\sqrt{g_\eta}+\nabla^2\sqrt{g_\eta}, \tag{3.8}$$

$$\sqrt{g_\eta}\partial_t\theta=2\nabla\sqrt{g_\eta}\cdot\nabla\theta+\sqrt{g_\eta}\nabla^2\theta, \tag{3.9}$$

where $1/C=\int dy[\tanh'(y)]^2/\int dy\ \tanh'(y)=\frac{2}{3}$. Applying the quasistatic assumption to $\sqrt{g_\eta}$ in Eq. (3.8), we obtain

$$1+\gamma-4\gamma g_\eta-Y_0^2q^2\approx C(\nabla\theta)^2, \tag{3.10}$$

where only the lowest-order term was taken into account. Substituting Eq. (3.10) into Eqs. (3.4) and (3.5), we obtain reduced equations as follows:

$$v_n = -\frac{1}{\sqrt{g_\eta}}\nabla\cdot\sqrt{g_\eta}\boldsymbol{n} = -\nabla\cdot\boldsymbol{n}(\boldsymbol{r},t) - \tfrac{1}{2}\boldsymbol{n}\cdot\nabla\ln g_\eta, \tag{3.11}$$

$$\partial_t q = \frac{Y_0^2}{2}(1-q^2)q + \frac{C}{2}(\nabla\theta)^2 q + \nabla^2 q - \frac{2}{\xi_B}\tanh(\eta/\xi_B)\nabla q\cdot\nabla\eta, \tag{3.12}$$

$$g_\eta = 1 + \frac{1-3\gamma}{4\gamma}(1-q^2) - \frac{C}{4\gamma}(\nabla\theta)^2, \tag{3.13}$$

where we have used $\partial_t\eta + \boldsymbol{v}\cdot\nabla\eta = 0$ in the frame moving with the interface in Eq. (3.4), and defined the normal component of the interface velocity $v_n \equiv v_n(\boldsymbol{r}(s,t))$.

Here the curvature of interface at the position $\boldsymbol{r}_0(s,t)$ is defined by

$$\kappa \equiv \kappa(\boldsymbol{r},t) = \nabla\cdot\boldsymbol{n}(\boldsymbol{r},t) = \nabla\theta\cdot\boldsymbol{t}(\boldsymbol{r},t). \tag{3.14}$$

Using the above and the relation $\nabla\theta = \kappa\boldsymbol{t}$ on the interface, we express $\nabla\cdot\boldsymbol{n}$ and $(\nabla\theta)^2$ in Eqs. (3.11), (3.12), and (3.13) with the curvature κ.

For later consideration, let us introduce a scaled local coordinate system $q(x',y',t) \equiv q(\zeta/\xi_0,\eta/\xi_B,t)$ instead of $q(x,y,t)$, where $\xi_0 (\equiv 2/Y_0)$ is the width of the wall connecting the opposite state of q, and has the meaning of the defect core size for the region $\xi_0 \ll \xi_B$. These coordinates are locally orthogonal to each other, and satisfy the formulas

$$\nabla q = \frac{\sqrt{g_\zeta}}{\xi_0}\boldsymbol{t}\partial_{x'}q + \frac{\sqrt{g_\eta}}{\xi_B}\boldsymbol{n}\partial_{y'}q, \tag{3.15}$$

$$\nabla^2 q = \frac{g_\zeta}{\xi_0^2}\partial_{x'}^2 q + \frac{g_\eta}{\xi_B^2}\partial_{y'}^2 q + \frac{1}{\xi_0}(\nabla\cdot\sqrt{g_\zeta}\boldsymbol{t})\partial_{x'}q + \frac{1}{\xi_B}(\nabla\cdot\sqrt{g_\eta}\boldsymbol{n})\partial_{y'}q, \tag{3.16}$$

$$g_\zeta \equiv \nabla\zeta\cdot\nabla\zeta, \nabla\zeta\cdot\nabla\eta = 0, \tag{3.17}$$

where one should note that the value of g_ζ is arbitrary chosen. Applying the above formulas and a relation $\nabla\cdot\boldsymbol{t} = 0$, which should be satisfied on the interface to Eq. (3.12), we obtain

$$\frac{\xi_0^2}{2}\frac{d}{dt}q = (1-q^2)q + \frac{C\xi_0^2\kappa^2}{4}q + \frac{g_\zeta}{2}\partial_{x'}^2 q + \frac{g_\eta}{2}\left(\frac{\xi_0}{\xi_B}\right)^2 \times\{\partial_{y'}^2 q - 2(\partial_{y'}q)\tanh(y')\}, \tag{3.18}$$

where we defined the time derivative dq/dt with respect to the coordinate moving with the interface by $(d/dt)q = \partial_t q - (1/\xi_B)(\nabla\cdot\sqrt{g_\eta}\boldsymbol{n})\partial_{y'}q$. By assuming that the curvature is sufficiently smooth and that the y' dependence of q can be neglected, the last term in Eq. (3.18) is ignored. Thus the reduced results are summarized as

$$\boldsymbol{v} = -\kappa\boldsymbol{n} - \nabla\ln(\sqrt{g_\eta}), \tag{3.19}$$

$$\frac{\xi_0^2}{2}\frac{d}{dt}q = (1-q^2)q + \frac{C\xi_0^2\kappa^2}{4}q + \tfrac{1}{2}\partial_{x'}^2 q, \tag{3.20}$$

$$g_\eta = 1 + \frac{2\xi_B^2}{\xi_0^2}(1-q^2) - \frac{C\xi_B^2}{2}\kappa^2, \tag{3.21}$$

where we chose $g_\zeta = 1$.

These results are interpreted as follows. The evolution of q obeys Eq. (3.20), and it is weakly coupled with the curvature. The fluctuation of q on the surface alters the width of wall through the factor $1/\sqrt{g_\eta}$, and makes some small correction to the interface velocity in addition to the main contribution from the surface tension. One will find that these results give no significant correction to the very familiar interface dynamics for the one-component TDGL system discussed below.

As mentioned above, the present system has two microscopic lengths: the defect core size ξ_0 and the interface width ξ_B. Because of this fact, two types of situation take place. Let us first consider the situation $\xi_0 \gg \xi_B$, where γ is close to $\frac{1}{3}$. From Eqs. (3.19) and (3.21), the interface velocity is given by $v_n \simeq -\kappa$. So the time development of the interface is driven by the curvature. By considering the quasiequilibrium state ($\dot{q} \approx 0$) without spatial variation ($\partial_{x'}^2 q \approx 0$), Eq. (3.20) gives $q^2 \sim 1 + C\xi_0^2\kappa^2/4$. The order parameter is thus written as $\psi \sim X[\eta/\xi_B] + i\sqrt{Y_0^2 + C\kappa^2}\,\mathrm{sech}(\eta/\xi_B)$. This means that the fluctuation of the interface suppresses the transition from the Bloch wall to the Ising wall. This result was checked by our numerical simulations.

Let us next consider the situation $\xi_0 \ll \xi_B$, where an interface description is still valid. In this case, one obtains $\xi_B^{-1} \gg \kappa$, and one must treat the two regions on the interface, (i) near defect ($q \sim 0$) and (ii) near the wall region ($q = q_0$, $q_0^2 \sim 1 + C\xi_0^2\kappa^2/4$), separately. Equation (3.21) is estimated as $g_\eta \sim 1 - C(\xi_B\kappa)^2$ for $q \sim q_0$, and $g_\eta \sim 1 + 2(\xi_B/\xi_0)^2[1 - (C/4)(\xi_0\kappa)^2] \sim 2(\xi_B/\xi_0)^2[1 - (C/4)(\xi_0\kappa)^2]$ for $q \sim 0$. Thus one obtains the interface velocity as

$$v_n \sim \begin{cases} -\kappa - C\xi_B^2\kappa^3 & \text{for } q \sim q_0 \\ -\kappa - \dfrac{C}{4}\xi_0^2\kappa^3 & \text{for } q \sim 0, \end{cases} \tag{3.22}$$

TABLE I. Dynamical exponent $l \sim t^z$ for the growth laws for the characteristic length scale for several values of γ. We measured this exponent numerically with the half-width length of the correlation function $C(r,t)$, utilizing least-squares regression.

γ	0.0	0.005	0.01	0.03	0.1	0.3	0.4
z	0.388	0.359	0.368	0.397	0.394	0.427	0.424
err.	0.005	0.003	0.005	0.014	0.007	0.011	0.007

where we used the relation $\boldsymbol{n}\cdot\nabla\kappa=\kappa^3$. This implies that the velocity of the interface depends on q, while it is small in comparison with $-\kappa$ due to the surface tension. One should note that when γ is sufficiently small, due to the divergence of ξ_B, the concept of the interface loses its validity, and instead we may have to use a dynamics based on a defect picture.

The above results imply the ordering process in the present system is mainly controlled by the surface tension, except in the early kinetic stage. Although we derived a correction to the interface velocity, due to the fluctuation of the chirality q, this has a minor correction. Therefore one finds the familiar result for the growth law $l(t)\sim t^z$ $(z=\frac{1}{2})$ derived from the dimensional analysis even in the present anisotropic spin system.

The dynamical exponents calculated from numerical results are shown in Table I, the method of the numerical calculation being explained before. We made a statistical average with 27 samples of different initial conditions.

IV. CORRELATION FUNCTION

In this section we discuss the equal time correlation function in the ordering process, which is defined $C(\boldsymbol{r},t)\equiv\langle\psi^*(\boldsymbol{x}+\boldsymbol{r},t)\psi(\boldsymbol{x},t)\rangle$, where the angular brackets indicate an average over the ensemble of possible initial conditions. It is known in the isotropic case that the correlation function has the scaling form $C(\boldsymbol{r},t)\equiv f(r/l(t))$ with the characteristic length $l(t)$. The scaling function $f(x)$ was obtained by Ohta, Jasnow, and Kawasaki [2] for the $O(1)$ system. Bray and Puri [4] and Toyoki [5] generalized it to the $O(n)$ system.

Being different from both the symmetric $O(2)$ and $O(1)$ systems, the present system has two length constants, ξ_B and ξ_0, in addition to $l(t)$. The former is the width of interface, and the latter plays the role of the defect core size for $\xi_0\ll\xi_B$.

For the situation $\xi_0\ll\xi_B$, one makes the scenario of the ordering process as follows. Once the system is quenched from the disordered state, the system experiences the nearly $O(2)$ symmetric phase for a short time, and then gradually converts to the $O(1)$ symmetric phase. In the first stage the order parameter's correlation is disturbed by the phase singularity from the defect when $l(t)$ is less than the width of interface $(l(t)\ll\xi_B)$, while in the second stage it is disturbed by the singularity from sharp interfaces when $l(t)$ exceeds ξ_B.

In the alternative situation $\xi_B\ll\xi_0$, after the quench the system gradually proceeds to the $O(1)$ symmetric phase, being associated by interface fluctuations. In the first situation we studied the crossover process to the ideal $O(1)$ symmetric phase by considering the contribution from interfaces.

To characterize the crossover process, one may utilize the short-scale behavior of the correlation function. It has been known that the correlation function represents features of the phase singularity of defects in a small-scale region. For one- and two-component systems in spatial dimensions larger than two, the scaling functions have been derived as [2,5,4,15],

$$f(z)\sim\begin{cases}1-\dfrac{2}{\pi}z & \text{at } n=1\\[2ex] 1-(\ln 2-\frac{1}{4}-\frac{1}{2}\ln z)z & \text{at } n=2.\end{cases}\tag{4.1}$$

Let us introduce the incomplete scaling function as $C(\boldsymbol{r},t)/\langle|\psi(\boldsymbol{x},t)|^2\rangle\sim f(r/l(t),l(t))$, which describes the crossover behavior of the scaling function. For the present purpose, it is convenient to rewrite function $f(r/l(t),l(t))$ as

$$f(r/l(t),l(t))\equiv 1-\tfrac{1}{2}\langle|\psi(\boldsymbol{x}+\boldsymbol{r},t)-\psi(\boldsymbol{x},t)|^2\rangle/\langle|\psi(\boldsymbol{x},t)|^2\rangle.\tag{4.2}$$

We evaluate this in two characteristic regimes, (A_I) $\xi_0\ll r\ll l(t)\ll\xi_B$ [nearly $O(2)$ regime], and (A_{II}) $\xi_0\ll\xi_B\ll r\ll l(t)$ [$O(1)$ regime]. Although there are situations (B_I) $\xi_B\ll r\ll l(t)\ll\xi_0$ and (B_{II}) $\xi_B\ll\xi_0\ll r\ll l(t)$ near the transition point from the Bloch wall to the Ising wall, we mainly discuss regimes A_I and A_{II} $(\xi_0\ll\xi_B)$.

One should note that the order-parameter difference at two different point $\boldsymbol{x},\boldsymbol{x}+\boldsymbol{r}$ in Eq. (4.2) consist of two parts, one of which is the contribution from ordered regions and another from defects or interfaces. The former is expressed by the Taylor expansion over a short distance. Thus one estimates

$$\text{2nd term in Eq. (4.2)}\sim\begin{cases}\dfrac{\langle||\nabla\psi||^2\rangle}{2\langle|\psi|^2\rangle}r^2\sim\dfrac{1}{l^2}\displaystyle\int_{\xi_0}^{l}dr'/r'r^2\sim\ln(l/\xi_0)(r/l)^2 & \text{for } A_I\\[2ex] \dfrac{\langle|\nabla X|^2\rangle+\langle|\nabla Y|^2\rangle}{2\langle|\psi|^2\rangle}r^2\sim 0 & \text{for } A_{II},\end{cases}\tag{4.3}$$

where, using a roughly estimation, we replaced the average with the integration of the order-parameter derivative over the ordered space, i.e., $\langle\cdots\rangle\sim\int' dr^d\ldots/l^d$ ($\int'$ implies that the integral range takes l^d space excluding a defect or an interface region). The latter cannot be expressed by the same expansion, due to the sharpness of the regions.

Let us express the difference in Eq. (4.2) by the weighted average of two contributions, and introduce the weights P_I and P_{II} as nonanalytic contributions for each regime of A_I and A_{II}. Here P_I and P_{II} represent the probabilities that the segment $\boldsymbol{r}$ intersects with a defect (A_I) and an interface (A_{II}), respectively. Therefore, both probabilities are roughly

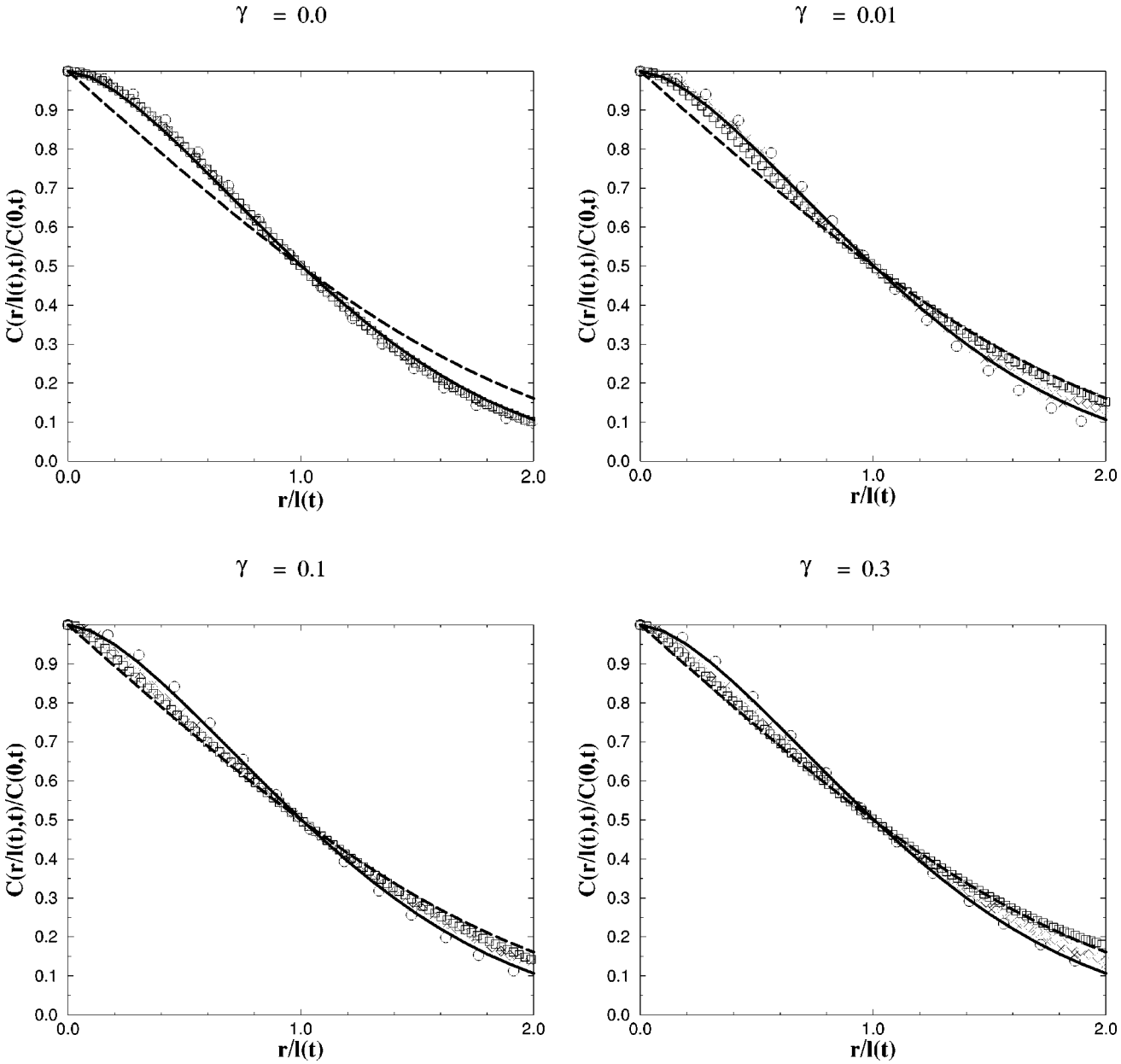

FIG. 3. Scaled correlation function $C(r/l,t)/C(0,t)$ for several γ values. The horizontal axis is scaled by the characteristic length generated by the half-width of the correlation function. Symbols correspond to times, $t=12$ (○), 152 (×), 452 (◇), and 1052 (□). Auxiliary lines represent form functions for the case $O(2)$, denoting $C_2(x)$ (solid), and for the case $O(1)$, denoting $C_1(x)$ (dashed), respectively.

estimated as $P_I \sim r^2/l^2$ and $P_{II} \sim rl/l^2 \sim r/l$, by considering a l^d volume which confines a defect or an interface within it.

Applying the order-parameter profile, Eq. (3.2), for Eq. (4.2), we obtain

$$f(r/l(t),l(t)) \sim \begin{cases} 1-[a_I P_I + (1-P_I) b_I \ln(l/\xi_0)(r/l)^2] & \text{for } A_I \\ 1-[a_{II} P_{II} + Q_{II} c_{II}] & \text{for } A_{II}. \end{cases} \tag{4.4}$$

Here $a_{I,II}$ indicate the order-parameter differences in the opposite phase, so it is a numerical factor of order 1, and b_I is a numerical factor of order 1. The last term $Q_{II}c_{II}$ represents the contribution from the wall region, and is defined as

$$Q_{II}c_{II} \equiv \frac{\langle [Y(\boldsymbol{x}+\boldsymbol{r},t)-Y(\boldsymbol{x},t)]^2 \rangle}{2\langle |\psi|^2 \rangle} \tag{4.5}$$

$$\sim \frac{Y_0^2}{X_0^2+Y_0^2} Q_{II} \langle [q(\boldsymbol{x}+\boldsymbol{r},t)-q(\boldsymbol{x},t)]^2 \rangle \tag{4.6}$$

$$\sim \frac{Y_0^2}{X_0^2+Y_0^2} \frac{\xi_B}{l} f_c(r/l(t)) \tag{4.7}$$

where $f_c(r/l(t)) \sim \langle [q(\boldsymbol{x}+\boldsymbol{r},t)-q(\boldsymbol{x},t)]^2 \rangle$, and Q_{II} represents the probability that the segment $\boldsymbol{r}$ exists within the interface, thus it is roughly estimated as $Q_{II} \sim \xi_B l/l^2 \sim \xi_B/l$.

Leaving from the region $\xi_B \gg \xi_0$, another time-scale fluctuation appears in the form $\langle [q(\boldsymbol{x}+\boldsymbol{r},t)-q(\boldsymbol{x},t)]^2 \rangle \sim (1+C\xi_0^2\kappa^2/4) f_c'(r/l)$, assuming a scaling function $f_c'(r/l)$. So we cannot scale the contribution from interfaces with single time scale over regions.

Summarizing the above results, we obtain the following forms:

$$f(r/l(t),l(t)) \sim \begin{cases} 1-(A_I+B_I-C_I \ln r/l)(r/l)^2 & \text{for I} \\ 1-A_{II}(r/l)-B_{II}(\xi_B/l) f_c(r/l) & \text{for II,} \end{cases} \tag{4.8}$$

where $A_{I,II}, B_{I,II}$, and C_I are numerical factors or other dimensionless correction reduced from complex integrals, which are not written as scaling form.

To summarize results of the scenario of the ordering process, it may be concluded that the correlation function behaves as $C(\boldsymbol{r},t) \sim \tilde{f}(r/l(t), \xi_B/l(t), \xi_0/l(t))$ generally, and that it decays simply to the $O(1)$ form with a time scale $\sim \xi_B/l(t)$ in a region $\xi_B \gg \xi_0$.

Next let us show the results of our numerical calculation. The method of numerical calculation was explained at the beginning of Sec. III. We made a statistical average with 27 samples of different initial conditions. Figure 3 shows the time development of the correlation function for several γ values. These figures are scaled with $l(t)$ obtained from each half-width value of it. Auxiliary lines drawn on the figures represent

$$f_1(x) = \frac{2}{\pi} \arcsin[\exp(-\ln 2/2x^2)] \quad \text{(dashed line)}, \tag{4.9}$$

$$f_2(x) = \frac{\pi}{4} s^{1/2} F(\tfrac{1}{2}, \tfrac{1}{2}, 2, s), \quad s = \exp(-x^2) \quad \text{(solid line)},$$

where the function F is the Gaussian hypergeometric function [5,8,9]. These functions are exact forms of Eq. (4.1). One can clearly find crossover behavior between both forms.

We characterize the asymptotic behavior of relaxation for the correlation function from the $O(2)$ form to the $O(1)$ one by defining a quantity that extracts the difference between a numerical result and the $O(1)$ correlation function as

$$D(t) = \int_0^\infty dx [f_1(x) - f(x, l(t))]^2. \tag{4.10}$$

From Eqs. (4.8) and (4.10), one finds the scaling form $D(t) \sim (\xi_B/l)^2 \sim (\gamma t)^{-1}$ in the region $\xi_B \gg \xi_0$, but, leaving from the region $\xi_B \gg \xi_0$, this form is disturbed by another time scale $\xi_0/l(t)$. Figure 4 shows the results for $D(t)$ for several values of γ (upper figure). $D(t)$ decays simply for nonzero γ as times goes on. The lower figure of Fig. 4 shows the scaling representation by $\tilde{D}(\gamma t)$. One can find the decay process $D(t) \sim (\gamma t)^{-1}$ except in the early kinetic stage for $\xi_B \gg \xi_0$ ($\gamma < 1/11$), and its violation for $\xi_0 \gg \xi_B$ ($\gamma > 1/11$), as we explained.

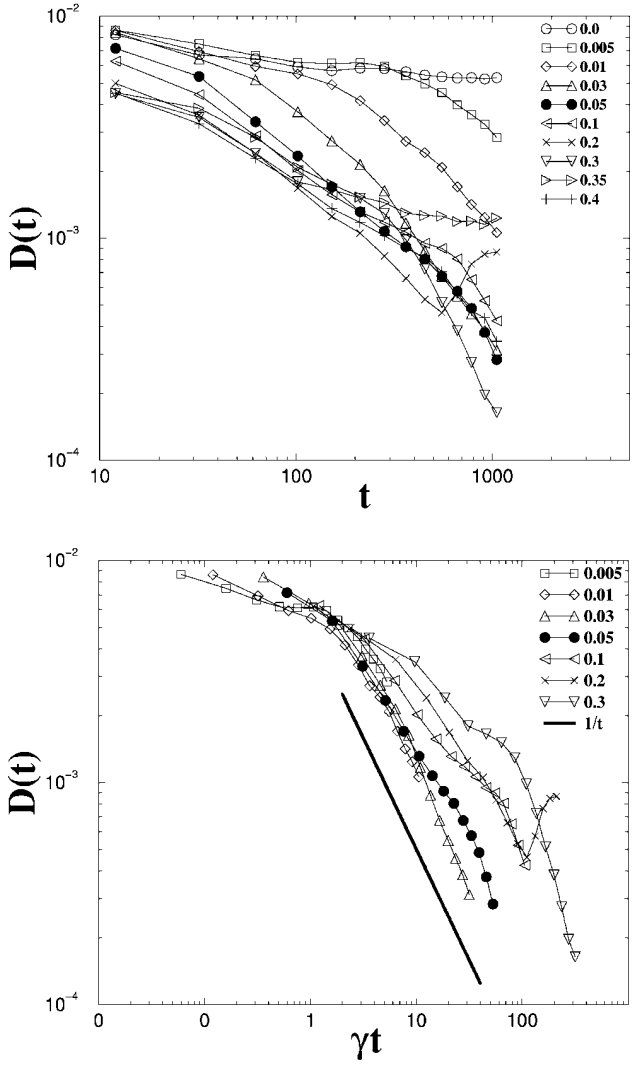

FIG. 4. Asymptotic behaviors of the correlation function vs time t calculated from Eq. (4.10). Numerical values in the figures are those for γ. $D(t)$ turns out to decay as $(\gamma t)^{-1}$ over a long time.

V. SUMMARY

In this paper we showed a nonconserved, purely dissipative, anisotropic XY system. This was done by first deriving evolution equations for the interface with chirality. The same argument can be easily extended to an anisotropic n-vector system with isotropic elasticity. We found a relation between interface width and the fluctuation of the chirality. When the wall width is shorter than the ordering length, the evolution is described by an Allen-Cahn-type equation weakly coupled with the amplitude of chirality.

We also investigated the crossover behavior of a correlation function in the small-scale region. Similar studies of the crossover behavior have recently been carried out. See, e.g., Ref. [16]. In the present system the crossover behavior was characterized by the width of the Bloch wall ξ_B and the time-dependent length scale $l(t)$, which characterizes the ordered region, even though there is another associative length constant ξ_0, which is the defect core size for $\xi_0 \ll \xi_B$, or the width of the wall for the chirality on the interface for ξ_0

$\gg \xi_B$. The crossover in the correlation function is seen by the magnitude of $l(t)/\xi_B$ in the limited situation $\xi_B \gg \xi_0$. We characterized the crossover by utilizing the difference of the correlation function from the ideal $O(1)$ function. We found the decay form for it by considering the contribution from interfaces, neglecting the correlation among defects in the nearly $O(2)$ regime. The prediction turned out to agree with the numerical result. In this estimation we used only the dimensionality of the defect and the space. This argument may be easily generalized into n-component systems. This will be reported in a near future.

ACKNOWLEDGMENTS

The author is grateful to H. Fujisaka for valuable discussion and a critical reading of the manuscript, and to H. Furukawa for helpful suggestions.

[1] A. N. Pargellis, P. Finn, J. W. Goodby, P. Panizza, B. Yurke, and P. E. Cladis, Phys. Rev. A **46**, 7765 (1992), and references therein.
[2] T. Ohta, D. Jasnow, and K. Kawasaki, Phys. Rev. Lett. **49**, 1223 (1982).
[3] A. D. Rutenberg and A. J. Bray, Phys. Rev. E **51**, 5499 (1995).
[4] A. J. Bray and Sanjay Puri, Phys. Rev. Lett. **67**, 2670 (1991).
[5] H. Toyoki, Phys. Rev. B **45**, 1965 (1992).
[6] G. F. Mazenko, Phys. Rev. E **49**, 3717 (1994); **50**, 3485 (1994).
[7] S. M. Allen and J. W. Cahn, Acta Metall. **27**, 1085 (1979).
[8] L. N. Bulaevskii and V. L. Ginzburg, Zh. Eksp. Teor. Fiz. **45**, 772 (1963) [Sov. Phys. JETP **18**, 530 (1964)].
[9] Y. Pomeau, Physica D **51**, 546 (1991).
[10] M. Kleman, in *Magnetism of Metals and Alloys*, edited by M. Cyrot (North-Holland, Amsterdam, 1982).
[11] P. Coullet and K. Emilsson, Physica D **61**, 119 (1992).
[12] H. Tutu and H. Fujisaka, Phys. Rev. B **50**, 9274 (1994).
[13] I. M. Lifshitz, Zh. Eksp. Teor. Fiz. **42**, 1354 (1962) [Sov. Phys. JETP **15**, 939 (1962)].
[14] K. Kawasaki and T. Ohta, Physica A **118**, 175 (1983).
[15] H. Tomita, Prog. Theor. Phys. **72**, 656 (1984).
[16] S. Puri, R. Ahluwalia, and A. J. Bray, Phys. Rev. E **55**, 2345 (1997).